Catalysis Science & Technology

Accepted Manuscript

This article can be cited before page numbers have been issued, to do this please use: S. U. Son, S. H. Ryu, S. J. Choi, J. H. Seon, B. Jo, S. M. Lee, H. J. Kim, Y. Ko, K. C. Ko and T. K. Ahn, *Catal. Sci. Technol.*, 2020, DOI: 10.1039/D0CY00997K.

ROYAL SOCIETY OF CHEMISTRY

rsc.li/catalysis

View Article Online
DOI: 10.1039/D0CY00997K

Journal Name

ARTICLE

Visible Light-Driven Suzuki-Miyaura Reactions by Self-Supported Pd Nanocatalysts in the Formation of Stille Coupling-Based Photoactive Microporous Organic Polymers

Received 00th January 20xx,
Accepted 00th January 20xx

DOI: 10.1039/x0xx00000x

www.rsc.org/

Sang Hyun Ryu,[a,‡] Sung Jae Choi,[a,‡] Ji Hui Seon,[b] Bonghyun Jo,[c] Sang Moon Lee,[d] Hae Jin Kim,[d] Yoon-Joo Ko,[e] Kyoung Chul Ko,*[b] Tae Kyu Ahn,*[c] and Seung Uk Son*[a]

Stille coupling was applied to synthesize microporous organic polymers (MOPs). Metallic Pd was *in situ* self-supported during the networking of 1,3,6,8-tetrabromopyrene with 1,4-bis(tributylstannyl)benzene to form Stille coupling-based MOP(St-MOP)@Pd. The size of St-MOP particles and the amount of metallic Pd in the St-MOP@Pd depended on the amount of a Pd catalyst. As the amount of a Pd catalyst increased, the size of St-MOP particles decreased with an increase of metallic Pd, due to the increased St-MOP nuclei in the early growth stage of St-MOP. The St-MOP bearing pyrenes showed absorption and emission of visible light and the St-MOP@Pd showed excellent catalytic performance in the visible light-driven Suzuki-Miyaura coupling. The optimal St-MOP@Pd-2 (0.14 mol% Pd) showed a TON of 657 and a TOF of 219 h^{-1} in the visible light-driven Suzuki-Miyaura coupling of 1-acetyl-4-bromobenzene and phenyl boronic acid at 25°C. The optimal amount of St-MOP and metallic Pd in the St-MOP@Pd was critical to achieve excellent catalytic performance. The overall photocatalytic principles of St-MOP@Pd were rationalized by computational simulation.

Introduction

Recently, various microporous organic polymers (MOPs) have been prepared by Pd-catalyzed couplings of organic building blocks.[1] Since conjugated microporous polymers (CMPs) were prepared by Cooper research group,[2] based on Sonogashira coupling of multihaloarenes with multiethynylarenes, there have been extensive studies on the synthesis and application of functional CMP.[1] In addition to Sonogashira coupling, other Pd-catalyzed coupling reactions have also been applied to prepare MOP. For example, Suzuki-Miyaura coupling and Heck reaction have been applied to synthesize MOP.[3,4] It is noteworthy that Stille coupling is a powerful synthetic method that doesn't require additional bases.[5] However, as far as we are aware, surprisingly, Stille coupling reaction has not been explored in the synthesis of MOP.

It has been well documented that conventional Pd-catalyzed coupling reactions follow Pd 0/+2 cycles.[6] During the catalytic cycles, molecular Pd species can be gradually decomposed to metallic Pd, the so called Pd black.[7] Usually, the formation of metallic Pd is regarded as an unwanted reaction pathway for Pd-catalyzed couplings because the uncontrolled Pd black has poor catalytic activity.[7] However, one can speculate that the gradual deposition of metallic Pd can be utilized for *in situ* loading of Pd nanoparticles (NPs) on solid supports.

The microporosity and the high surface areas of MOP are beneficial features in its use as a solid support for the Pd loading. In this regard, MOP@Pd materials have been prepared and applied to heterogeneous Pd catalysis.[8] However, in the conventional synthesis of MOP@Pd materials, metallic Pd was additionally deposited on pre-synthesized MOP using Pd precursors.[8] Regarding pot economy,[9] one pot synthesis of MOP@Pd will be more attractive. One can expect that the metallic Pd can be *in situ* deposited in the synthetic process of MOP to form MOP@Pd materials in a one pot manner. Moreover, the amount of metallic Pd in the MOP materials can be systematically controlled *via* quantitative control of Pd catalysts. In addition, the size of MOP materials can be controlled by kinetic growth control using Pd catalysts. For example, as the amount of Pd catalysts increases, the number of MOP nuclei may increase in the early growth stage of MOP, resulting in a size decrease of the MOP materials.[10] Our research group has reported that the size and morphology engineering of MOP materials is important in their application.[11]

[a] *Department of Chemistry, Sungkyunkwan University, Suwon 16419, Korea E-mail: sson@skku.edu*
[b] *Department of Chemistry Education, Chonnam National University, Gwangju 61186, Korea E-mail: kcko1982@jnu.ac.kr*
[c] *Department of Energy Science, Sungkyunkwan University, Suwon 16419, Korea E-mail: taeahn@skku.edu*
[d] *Korea Basic Science Institute, Daejeon 34133, Korea*
[e] *Laboratory of Nuclear Magnetic Resonance, NCIRF, Seoul National University, Seoul 08826, Korea*

† Electronic Supplementary Information (ESI) available: Additional characterization data of St-MOP@Pd materials. See DOI: 10.1039/x0xx00000x

‡ These authors contributed equally.

Recently, visible light has been recognized as a sustainable energy source not only in the generation of electricity[12] but also in organic synthesis.[13] Visible light-induced cross-coupling by the combination of Pd catalysts with visible light-harvesting materials has been an important research subject.[14] For example, surface plasmonic nanomaterial@Pd systems[15] and *g*-C_3N_4@Pd[16] have been utilized as catalytic systems for the visible light-driven Suzuki-Miyaura coupling reactions. In addition, visible light-absorbing MOP@Pd can be applied as catalysts to the visible light-driven cross coupling reactions.[17] In this work, we report one pot synthesis of visible light active MOP@Pd materials based on Stille coupling (St-MOP@Pd) and their excellent photocatalytic performance in the visible light-driven Suzuki-Miyaura coupling reactions.

Experimental

General Information

Scanning electron microscopy was conducted using a FE-SEM (JSM6700F). Transmission electron microscopy was conducted using a JEOL 2100F. N_2 sorption isotherm curves were obtained at 77K using a Micromeritics ASAP2020. Pore size distribution diagrams were analyzed by the density functional theory method. Infrared spectra were obtained using a Bruker VERTEX 70 FT-IR spectrometer. Solid state ^{13}C nuclear magnetic resonance (NMR) spectra were obtained at CP/TOSS mode using a 500 MHz Bruker ADVANCE II NMR spectrometer. A 4 mm magic angle spinning probe and a spinning rate of 5 kHz were applied. Solution state ^1H NMR spectra were obtained using a 400 MHz and 500 MHz Varian spectrometers. Power X-ray diffraction patterns were obtained using a Rigaku MAX-2200 (filtered Cu-Kα radiation). X-ray photoelectron spectra were obtained using a Thermo VG equipment. Diffuse reflectance spectra were obtained using a Shimadzu UV-3600. UV/vis absorption spectra of St-MOP@Pd materials were obtained through the conversion of the corresponding diffuse reflectance spectra. Emission spectra were obtained using a JASCO FP-6200. Inductively coupled plasma-atomic emission spectroscopy was conducted using an OPTIMA 8300. Thermogravimetric analysis was conducted under N_2 using a Seiko Exstar 7300 analyzer.

Synthesis of St-MOP@Pd materials

For the preparation of St-MOP@Pd-1, $(PPh_3)_4Pd$ (2.3 mg, 2.0 μmol) and distilled DMF (60 mL) were added to a 150 mL flame-dried Schlenk flask under argon. The reaction mixture was sonicated for 30 min. After 1,3,6,8-tetrabromopyrene (62 mg, 0.12 mmol) and 1,4-bis(tributylstannyl)benzene (0.14 mL, 0.24 mmol) were added, the reaction mixture was stirred at 110°C for 24 h. After being cooled to room temperature, the resultant powder was separated by centrifugation, washed with methanol (40 mL) three times, methylene chloride (40 mL) three times, and dried under vacuum. For the preparation of St-MOP@Pd-2, the same synthetic procedures of St-MOP@Pd-1 were applied except using $(PPh_3)_4Pd$ (4.6 mg, 4.0 μmol). For the preparation of St-MOP@Pd-3, the same synthetic procedures of St-MOP@Pd-1 were applied except using $(PPh_3)_4Pd$ (9.2 mg, 8.0 μmol).

Experimental procedures for catalytic reaction

Aryl bromide (0.500 mmol), aryl boronic acid (0.625 mmol), St-MOP@Pd-2 (9.0 mg, 0.831wt% Pd, 0.14 mol% Pd), K_2CO_3 (0.104 g. 0.750 mmol), and methanol (3 mL) were added to a test tube under argon. The reaction temperature was kept at 25°C using a circulated water bath. After white LED (light intensity of 0.9 mW/cm^2 measured on the surface of a glass ware) was irradiated, the reaction progress was monitored by ^1H NMR studies. As a control system of dark conditions, the test tube was wrapped with an aluminum foil and a black insulating tape. For the catalytic reactions of other St-MOP@Pd catalysts, St-MOP@Pd-1 (35.9 mg, 0.203wt% Pd, 0.14 mol% Pd) and St-MOP@Pd-3 (5.7 mg, 1.34wt% Pd, 0.14 mol% Pd) were used.

For the recyclability tests, after reaction, the St-MOP@Pd-2 was recovered by centrifugation, washed with a mixture of distilled water (15 mL) and methanol (15 mL) three time and a mixture of methanol (10 mL), acetone (10 mL), and methylene chloride (10 m) three times, dried under vacuum, and used for the next run.

Laser photophysics

Time-resolved photoluminescence curves were obtained using a commercial TCSPC system (FluoTime 200, PicoQuant). A picosecond diode laser of 485 nm (LDH-P-C-485, PicoQuant) was used to excite St-MOP@Pd materials in methanol (a repetition rate of 4 MHz, an incident angle of 30°). The photoluminescence signals at 520 nm were accumulated by a fast photomultiplier tube (PMT) detector (PMA 182, PicoQuant) with an optimized angle (54.7°). The channels per a curve were set to 6250. The instrumental response function (IRF) was 160 ps in a full width at half maximum. We used convoluting decay curves to calculate decay lifetime using exponential functions; τ_{avg}(amplitude weighted average lifetime) = $A_1\exp(-t/\tau_1)$ + $A_2\exp(-t/\tau_2)$, A_1 and A_2: amplitude, τ_1 and τ_2: life time, t: time. The fitted values of the goodness-of-fit parameter (χ^2) were all close to 1.0.

Computational Simulation

The density functional theory (DFT) calculations were carried out using FHI-aims code.[18] We designed four model systems of St-MOP-I, II, III, and ∞ (Refer to Fig. 6a) to simulate the valence band (VB) and conduction band (CB) energy levels. For St-MOP-I, II, and III, the B3LYP/light-tier-1 level of theory was employed for the DFT calculation. For ∞, the PBE/light-tier-1 level of theory was used for the optimization of atomic position as well as unit cell parameters. A k-point grid was chosen as 7 × 7 × 7. The unit cell parameters of St-MOP-∞ were optimized as a = 14.56 Å, b = 17.95 Å, and c = 45.51 Å. The slab was separated by a vacuum spacing of 40 Å along with c axis to avoid the interaction between slabs within periodic boundary condition. After the geometrical optimization of St-MOP-∞ with a PBE function, single point calculation with B3LYP/light-tier-1 was performed to obtain the VB and CB energy levels. Considering computational costs, the convergence criteria for structure optimizations were set to 0.01 eV/Å for St-MOP-I and St-MOP-II, and as 0.02 eV/Å for St-MOP-III and St-MOP-∞, respectively.

Result and Discussion

Fig. 1 shows a synthetic scheme for the St-MOP@Pd. Using 1 eq. 1,3,6,8-tetrabromopyrene and 2 eq. 1,4-bis(tributylstannyl)benzene as building blocks, Stille coupling was conducted at 110°C in DMF for 24 h in the presence of tetrakis(triphenylphosphine)palladium(0). We systematically increased the amount of Pd catalysts from 1.7 mol% to 3.3 and 6.6 mol% of 1,3,6,8-tetrabromopyrene and the resultant materials were denoted as St-MOP@Pd-1, St-MOP@Pd-2, and St-MOP@Pd-3, respectively. When we used 1.7 mol% Pd catalyst of 1,3,6,8-tetrabromopyrene, greenish yellow powder was obtained. As the amount of Pd catalysts increased to 3.3 and 6.6 mol% of 1,3,6,8-tetrabromopyrene, the color of powders became darker and darker.

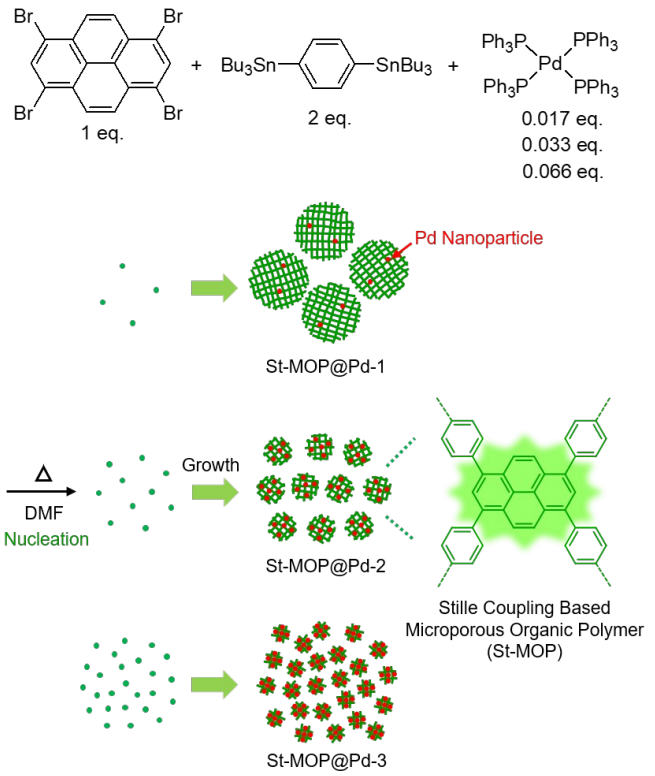

Fig. 1 One pot synthesis of St-MOP@Pd based on Stille coupling.

Scanning electron microscopy (SEM) showed that all St-MOP@Pd materials have spherical shapes. (Fig. 2a-c) Their average diameters decreased from 556 nm (St-MOP@Pd-1) to 192 nm (St-MOP@Pd-2) and 117 nm (St-MOP@Pd-3). Transmission electron microscopy (TEM) showed that the St-MOP particles were decorated with metallic Pd NPs with sizes of 1 ~ 3 nm. (Fig. 2d-i) Whilst Pd NPs were hardly detected in the St-MOP@Pd-1, a significant amount of Pd NPs was observed on the St-MOP of the St-MOP@Pd-2. (Fig. 2g-h) In the case of St-MOP@Pd-3, the St-MOP particles were coated with excess Pd NPs. (Fig. 2i and S1 in the ESI) The amounts of Pd were analyzed to be 0.203, 0.831, and 1.34wt% in the St-MOP@Pd-1, St-MOP@Pd-2, and St-MOP@Pd-3, respectively, by the inductively coupled plasma-atomic emission spectroscopy (ICP-AES).

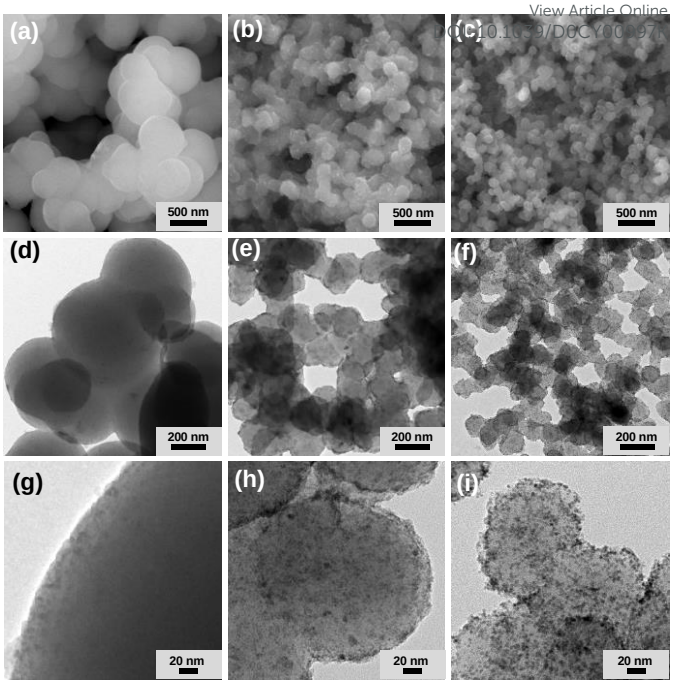

Fig. 2 SEM images of (a) St-MOP@Pd-1, (b) St-MOP@Pd-2, and (c) St-MOP@Pd-3. TEM images of (d, g) St-MOP@Pd-1, (e, h) St-MOP@Pd-2, and (f, i) St-MOP@Pd-3. Also, refer to Fig. S1 in the ESI.

The surface areas of St-MOP@Pd materials were characterized by the analysis of N_2 adsorption-desorption isotherm curves, based on the Brunauer-Emmett-Teller theory. (Fig. 3a-b) The St-MOP@Pd-1 showed a surface area of 32 m^2/g and poor porosity, which is attributable to the incomplete networking. (Also, refer to the analysis of ^{13}C NMR spectrum of St-MOP@Pd-1 in Fig. 3e) In comparison, the surface area of St-MOP@Pd-2 increased to 341 m^2/g with enhanced microporosity. Because of the increased amount of Pd NPs, the surface area of St-MOP@Pd-3 decreased to 285 m^2/g, compared to that of St-MOP@Pd-2. (Fig. 3a-b)

The chemical structures of St-MOP@Pd materials were characterized by X-ray photoelectron spectroscopy (XPS), infrared (IR) absorption, and solid state ^{13}C nuclear magnetic resonance (NMR) spectroscopy. (Fig. 3c-e) The XPS spectra of all St-MOP@Pd materials showed Pd 3d orbital peaks at 335.4 and 340.8 eV, corresponding to zerovalent Pd species.[19] (Fig. 3c) Additional Pd 3d orbital peaks were observed at 337.0 and 342.4 eV in the XPS spectrum of St-MOP@Pd-3, indicating the formation of PdO species on the surface of Pd NPs through partial surface oxidation.[19] (Fig. 3c) The IR absorption spectra of St-MOP@Pd materials showed the vibration peaks of aromatic C-H and oop C-H at 3035 and 833 cm^{-1}, respectively. (Fig. 3d) The aromatic C=C stretching peaks were observed at 1593, 1481, and 1460 cm^{-1}. In addition, aliphatic C-H stretching peaks were observed at 2952, 2922, and 2859 cm^{-1}, corresponding to tributylstannyl groups in the materials. The IR intensities of the tributylstannyl groups gradually decreased from St-MOP@Pd-1 to St-MOP@Pd-2 and St-MOP@Pd-3, indicating the enhanced progress of networking due to the increased Pd catalysts. (Fig. 3d)

The solid state ^{13}C NMR spectra of all St-MOP@Pd materials showed the aromatic ^{13}C peaks at 139, 136, and 127 ppm. (Fig. 3e) In addition, the aliphatic ^{13}C peaks of tributylstannyl groups were observed at 26 and 12 ppm. The intensity of the aliphatic ^{13}C peaks gradually decreased from St-MOP@Pd-1 to St-MOP@Pd-2 and St-MOP@Pd-3, matching well with the results of IR spectroscopy. (Fig. 3e)

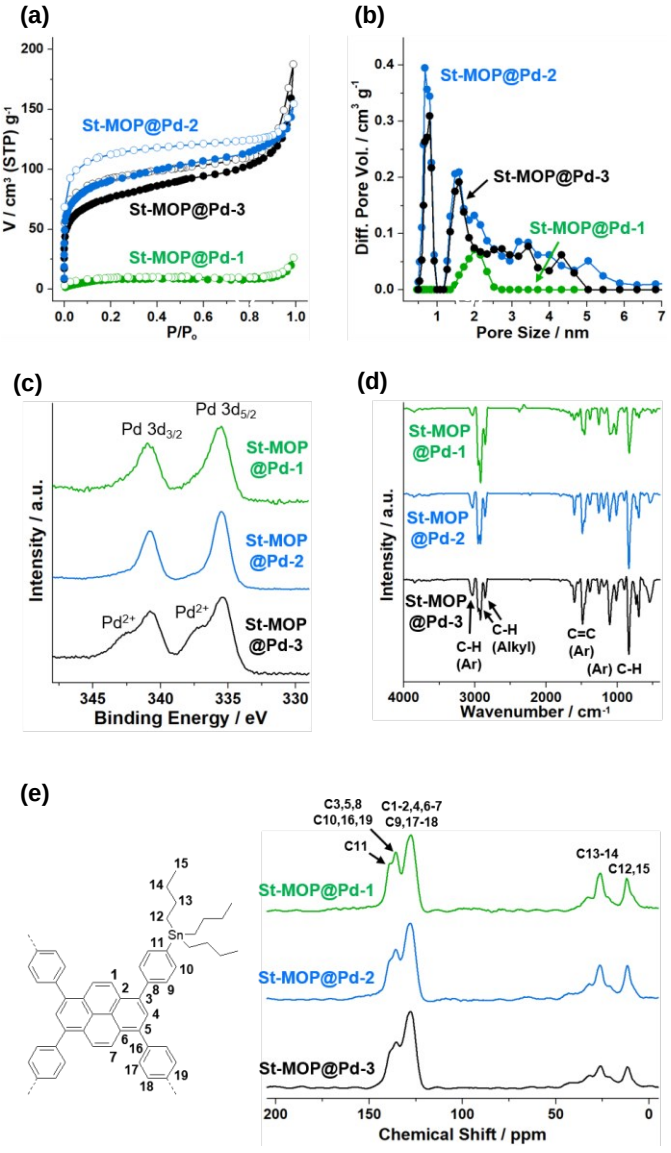

Fig. 3 (a) N_2 adsorption-desorption isotherm curves obtained at 77K, (b) pore size distribution diagrams based on the DFT method, (c) XPS spectra of Pd 3d orbitals, (d) IR absorption spectra, and (e) solid state ^{13}C NMR spectra of St-MOP@Pd-1, St-MOP@Pd-2, and St-MOP@Pd-3.

Powder X-ray diffraction (PXRD) studies showed that the St-MOP@Pd-1 is amorphous, matching with the conventional features of MOP materials prepared by the Pd-catalyzed cross-coupling reactions in the literature.[1-2] (Fig. S2 in the ESI) In the PXRD patterns of the St-MOP@Pd-2 and St-MOP@Pd-3, broad XRD peaks appeared at 2θ of 40.0°, corresponding to the (111) crystal plane of metallic Pd. (Fig. S2 in the ESI)

The optical properties of St-MOP@Pd were investigated. (Fig. 4) As shown in Fig. 4a, St-MOP@Pd-1 and St-MOP@Pd-2 showed three ultraviolet absorption bands at 247, 290, and 360 nm. In the visible light region, the St-MOP@Pd-1 and St-MOP@Pd-2 showed absorption bands at 450 and 454 nm, respectively. In the case of St-MOP@Pd-3, the intensities of absorption at 247, 290, and 360 nm were significantly reduced, due to the reduced amount of St-MOP in the materials, and the absorption at ~450 nm was not clearly observed. Instead, absorption was observed over the whole visible light region, due to the black Pd NPs in the St-MOP@Pd-3.

When the St-MOP@Pd-1 was excited with an excitation wavelength of 450 nm, it showed strong emission at 522 nm. (Fig. 4b) In comparison, the emission was significantly reduced in the excitation of St-MOP@Pd-2 and St-MOP@Pd-3, indicating the photo-induced electron transfer from St-MOP to Pd NPs. When the Pd NPs in St-MOP@Pd-2 was etched by the treament with HCl solution, the resulatnt St-MOP showed strong emission at 533 nm. The emission quantum yield of St-MOP of St-MOP@Pd-2 was measured to be 53.1% using $[Ru(bpy)_3](PF_6)_2$ as a standard compound.[20] The emission decay kinetics of the St-MOP@Pd materials were investigated by laser photophysics. (Fig. 4c) As the amount of Pd increased from St-MOP@Pd-1 to St-MOP@Pd-2 and St-MOP@Pd-3, the average lifetimes of emission gradually decreased from 0.94 ns to 0.37 and 0.34 ns, respectively, indicating the photo-induced electron transfer from the excited St-MOP to Pd NPs. As shown in Fig. 4d, whilst the St-MOP@Pd-1 in methanol showed bright emission, the emission of St-MOP@Pd-2 and the St-MOP@Pd-3 was gradually quenched by the Pd NPs in the materials.

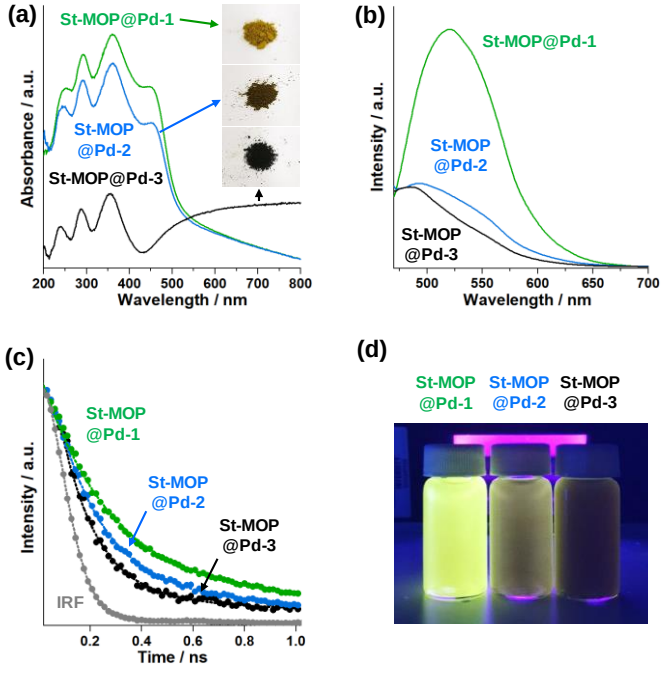

Fig. 4 (a) Absorption spectra (inset: photographs) of St-MOP@Pd-1, St-MOP@Pd-2, and St-MOP@Pd-3 powder. (b) Emission spectra (λ_{ex}: 450 nm), (c) emission decay curves, and (d) photographs of St-MOP@Pd-1, St-MOP@Pd-2, and St-MOP@Pd-3 in methanol.

Considering the possible visible light-induced electron transfer from St-MOP to Pd NPs, we studied the photocatalytic performance of St-MOP@Pds in the visible light-driven Suzuki-Miyaura coupling. We maintained reaction temperature to 25ºC using a circulated water bath. Also, as a control system for dark conditions, reactors were wrapped with an aluminum foil and an insulating tape. Fig. 5 summarizes the results. When we used 1-acetyl-4-bromobenzene and phenyl boronic acid as substrates of Suzuki-Miyaura coupling, the SMOP@Pd-2 showed sharp difference in the yields of products with/without white LED irradiation. (Fig. 5a) After 3 h, whilst the St-MOP@Pd-2 (0.14 mol%) showed a 92% yield of a coupled product under white LED irradiation, a 40% yield was obtained under dark conditions. When the Pd NPs of St-MOP@Pd-2 were etched through acid treatment, the system lost the original photocatalytic activities under white LED irradiation. (Fig. S3 in the ESI) When the St-MOP@Pd-2 was removed from a reaction mixture through filtration, the photocatalytic reaction was nearly terminated. (Fig. S4 in the ESI)

In comparison, the St-MOP@Pd-3 (0.14 mol% Pd) showed moderate conversions both under white LED irradiation (42% after 5 h) and under dark conditions (31% after 5 h), due to the blocking of visible light absorption by the excess Pd NPs on the surface of St-MOP. (Fig. 5a) The St-MOP@Pd-1 (0.14 mol% Pd) also showed poor conversions both under white LED irradiation (13% after 5 h) and under dark conditions (10% after 5 h), due to the diluted and entrapped Pd NPs in the materials and poor porosity. (Fig. 5a) These results indicate that the optimal amount between light absorbing materials (St-MOP) and Pd NPs is critical to be an efficient photocatalytic system for visible light-driven Suzuki-Miyaura coupling.

Next, we studied the substrate effect of arylbromides and arylboronic acids. (Fig. 5b-c) To be successful visible light-driven Suzuki-Miyaura coupling, the energy level of the conduction band (CB) of visible light-harvesting St-MOP should be higher than that of the LUMO of arylbromide substrates.[14-17] In addition, the energy level of the valence band (VB) of St-MOP should be lower than that of the HOMO of arylboronic acid or arylborate substrates. Thus, the electron deficient arylbromides and electron rich arylboronic acids can be good substrates for the visible light-driven coupling. Thus, we tested various aryl bromides with phenyl boronic acid for the visible light-driven coupling.

Among aryl bromides, 1-acetyl-4-bromobenzene and 1-bromo-4-formylbenzene showed successful conversions (92% and 81% yields, respectively, after 3 h) in the visible light-driven Suzuki-Miyaura coupling by St-MOP@Pd-2 (0.14 mol% Pd), compared to the poor results (40% and 26% yields, respectively, after 3 h) under dark conditions. Whilst the 1-bromo-4-nitrobenzene showed fast conversion (100% after 0.5 h) under white LED irradiation, the reaction under dark condition also became relatively slow (24% after 0.5 h). As the electronic surrounding of aromatic rings of arylbromides became more electron-rich, the yields of products gradually decreased. Whilst the bromobenzene and 1-bromo-4-methoxybenzene showed 51% and 12% yields after 5 h under white LED irradiation, they showed 25% and 0% yields, respectively, after 5 h under dark conditions. The poor conversions are attributable to the inefficient photo-induced electron transfer from the St-MOP to bromobenzene and 1-bromo-4-methoxybenzene.

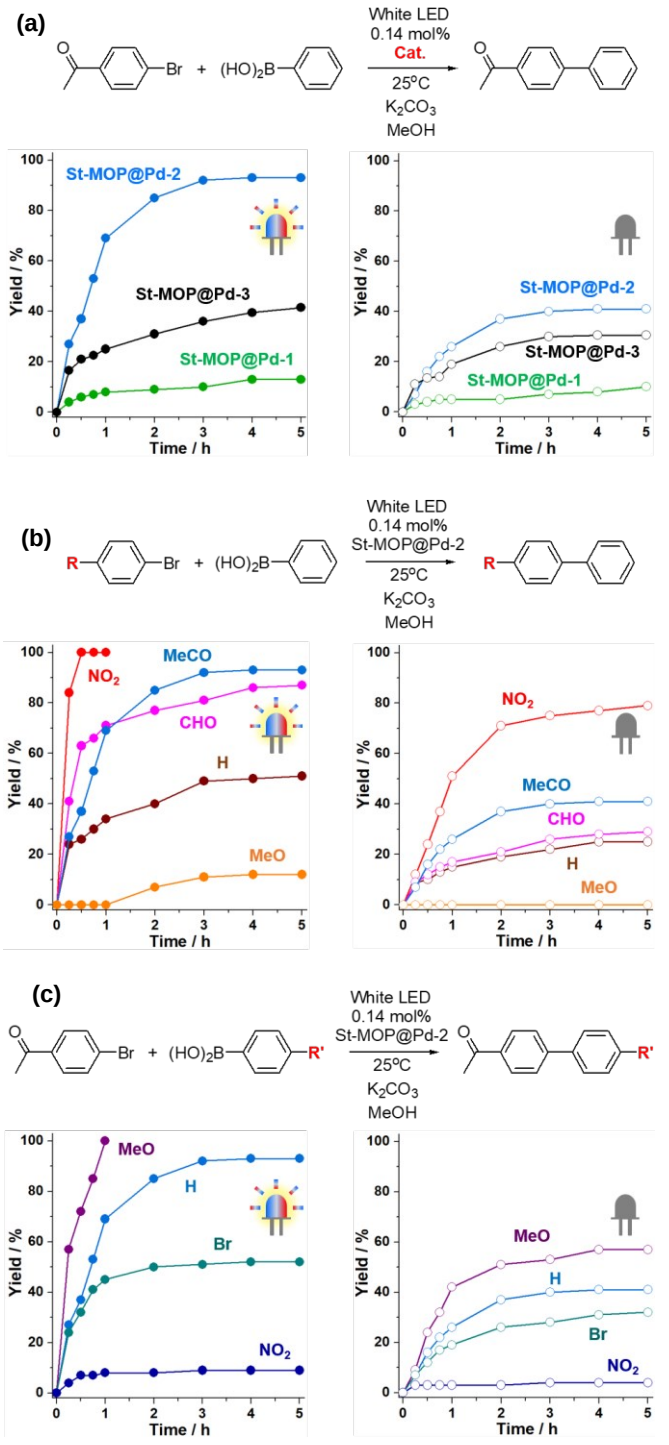

Fig. 5 Visible light-driven Suzuki-Miyaura coupling reactions (solid circle), compared to those under dark conditions (blank circle) depending on (a) catalysts (St-MOP@Pd), (b) aryl bromides, and (c) aryl boronic acids. Reaction condition: 0.14 mol% Pd, aryl bromide (0.500 mmol), aryl boronic acid (0.625 mmol), K_2CO_3 (0.750 mmol), 25ºC, MeOH, white LED irradiation (0.9 mW/cm²).

Next, we tested the effect of aryl boronic acids with 1-acetyl-4-bromobenzene in the visible light-driven Suzuki-Miyaura coupling. (Fig. 5c) As the electronic surroundings of aryl boronic acids became more electron-rich, the visible light-driven Suzuki-Miyaura coupling was enhanced. Whilst 4-methoxyphenylboronic acid showed a 100% yield by St-MOP@Pd-2 (0.14 mol% Pd) after 1 h under white LED irradiation, it showed a 42% yield after 1 h under dark conditions. Whilst phenylboronic acid showed 92% yield after 3 h under white LED irradiation, it showed a 40% yield after 3 h under dark conditions. 4-Bromophenylbronic acids showed a moderate yield of 52% after 5 h under white LED irradiation (a 32% yield after 5 h under dark conditions). 4-Nitrophenylbronic acid showed a poor yield of 9% after 5 h under white LED irradiation (a 4% yield after 5 h under dark conditions).

The substrate dependency of visible light-driven Suzuki-Miyaura coupling by St-MOP@Pd was rationalized by computational simulation. (Fig. 6a and S5-6 in the ESI)

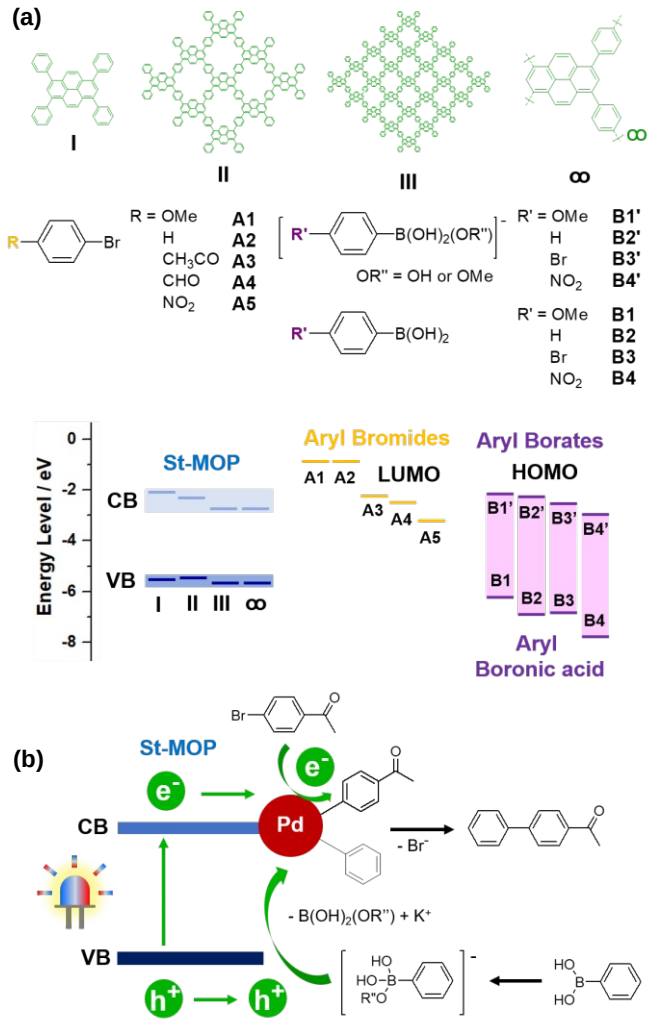

Fig. 6 (a) Model systems for the simulation, simulated conduction band (CB) and valence band (VB) energy levels of St-MOP, and HOMO and LUMO energy levels of aryl bromides, aryl boronic acids, and aryl borates. (b) A possible reaction mechanism of visible light-driven Suzuki-Miyaura coupling by St-MOP@Pd.

As denoted by I, II, III, and ∞ in Fig. 6a, the model systems of St-MOP were simulated through a systematic extending of conjugation lengths. According to the density functional theory (DFT) calculation, the CB and VB energy levels of St-MOP were simulated at -2.05 ~ -2.70 and -5.41 ~ -5.60 eV, respectively. (Fig. 6a and Table S1 in the ESI) The LUMO energy levels of 1-bromo-4-methoxybenzene, bromobenzene, 1-acetyl-4-bromobenzene, 1-bromo-4-formylbenzene, and 1-bromo-4-nitrobenzene were simulated at -0.80, -0.83, -2.19, -2.44, and -3.13 eV, respectively, indicating that the 1-acetyl-4-bromobenzene, 1-bromo-4-formylbenzene, and 1-bromo-4-nitrobenzene with the LUMO energy levels similar to or lower than the CB energy level of St-MOP can act as electron acceptors of the photo-excited St-MOP, matching well with the experimental results.

The HOMO energy levels of 4-methoxyphenylboronic acid, phenylboronic acid, 4-bromophenylboronic acid, and 4-nitrophenylboronic acid were simulated at -6.22, -6.96, -6.82, and -7.78 eV, respectively. (Fig. 6a and Table S1 in the ESI) It is noteworthy that that aryl boronic acids can be converted to aryl borates in the presence of bases.[21] The HOMO energy levels of the trihydroxyborate forms of 4-methoxyphenylboronic acid, phenylboronic acid, 4-bromophenylboronic acid, and 4-nitrophenylboronic acid were simulated at -2.08, -2.22, -2.49, and -2.91 eV, respectively. Those of dihydroxymethoxyborate forms of 4-methoxyphenylboronic acid, phenylboronic acid, 4-bromophenylboronic acid, and 4-nitrophenylboronic acid were simulated at -2.07, -2.15, -2.42, and -2.82 eV, respectively. In addition, those of dihydroxycarbonatoborate forms of 4-methoxyphenylboronic acid, phenylboronic acid, 4-bromophenylboronic acid, and 4-nitrophenylboronic acid were simulated at 2.32, 2.35, 2.11, and 1.79 eV, respectively. The HOMO energy levels of aryl borates are higher than the VB energy levels of St-MOP, indicating that these species can act as electron donors to the holes of the VB band of excited St-MOP. As the chemical surrounding of arylborates became more electron-rich, their HOMO energy levels are located higher, resulting in the enhanced electron donor ability.

The photocatalytic mechanism of the visible light-driven Suzuki-Miyaura coupling by St-MOP@Pd-2 was displayed as Fig. 6b. The St-MOP absorbs the visible light and then, the excited electron is transferred to arylbromide through Pd NP to generate an aryl moiety on the Pd NP and a free bromide anion. The arylborate donates electron to quench the hole of the VB of the St-MOP. The aryls on the Pd NP are coupled to form the Suzuki-Miyaura cross-coupled product. The substrate selectivity originates from the proper energy level location between the CB of St-MOP and the LUMO of arylbromides.

According to thermogravimetric analysis, the St-MOP@Pd-2 was thermally stable up to 201°C. (Fig. 7a) The recyclability of St-MOP@Pd-2 was investigated for visible light-driven Suzuki-Miyaura coupling of 1-acetyl-4-bromobenzene and phenylboronic acid. (Fig. 7b) In the first, second, third, fourth, and fifth runs, the St-MOP@Pd-2 (0.14 mol% Pd) showed excellent yields of 93, 93, 92, 90, and 90%, respectively. The St-MOP@Pd-2 recovered after five successive recycle tests

View Article Online
DOI: 10.1039/D0CY00997K

were investigated by SEM, XPS, and IR spectroscopy, showing the complete retention of the original morphology and chemical structure. (Fig. 7c-d and S7 in the ESI)

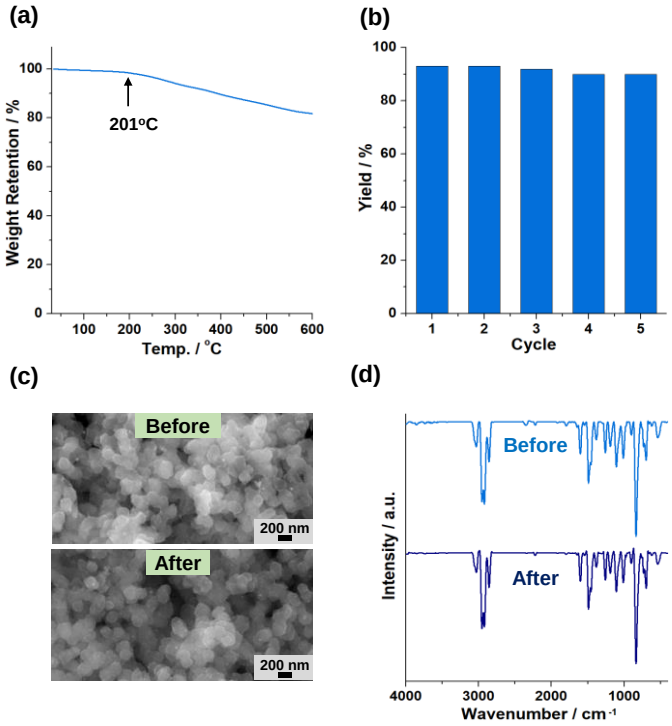

Fig. 7 (a) A TGA curve of St-MOP@Pd-2. (b) Recyclability tests of St-MOP@Pd-2 (0.14 mol% Pd) in the visible light-driven Suzuki-Miyaura coupling. Reaction conditions: 1-acetyl-4-bromobenzene (0.500 mmol), phenylboronic acid (0.625 mmol), K_2CO_3 (0.750 mmol), MeOH, 25°C, 5 h, white LED irradiation (0.9 mW/cm^2). (c) SEM images and (d) IR spectra of St-MOP@Pd-2 before and after five recyclability tests.

The photocatalytic performance of the optimal St-MOP@Pd-2 can be compared with those of recent polymer@Pd materials in the literature.[16-17] (Table S2 in the ESI) At first, Li and coworkers reported that *g*-C_3N_4@Pd (1.87 mol% Pd) showed a 97% yield in the visible light-driven Suzuki-Miyaura coupling of iodobenzene with phenylboronic acid at 25°C for 1 h, corresponding to a TON of 52 and a TOF of 52 h^{-1}.[16] Zhang and coworkers prepared conjugated microporous poly(benzoxadiazole) network with Pd NPs (0.56 mol% Pd), showing a 96% yield in the visible light-driven Suzuki-Miyaura coupling of 1-bromo-4-fluorobenzene with phenylboronic acid at room temperature after 4 h, corresponding to a TON of 171 and a TOF of 43 h^{-1}.[17a] The same catalyst showed a 76% yield in the reaction of 1-acetyl-2-bromobenzene with phenylboronic acid at room temperature for 16 h, corresponding to a TON of 136 and a TOF of 8 h^{-1}.[17a]

Polydopamine nanofilms with Pd NPs (0.56 mol% Pd) prepared by Xie, Wang, and coworkers showed a 95% yield in the visible light-driven Suzuki-Miyaura coupling of methyl 4-bromobenzoate with phenylboronic acid at room temperature for 2 h, corresponding to a TON of 170 and a TOF of 85 h^{-1}.[17b] Recently, Li, Lang, and coworkers prepared conjugated nanoporous polycarbazole with Pd NPs (0.50 mol% Pd), showing a 85% yield in the visible light-driven Suzuki-Miyaura coupling of 1-acetyl-4-chlorobenzene with phenylboronic acid at room temperature for 48 h, corresponding to a TON of 170 and a TOF of 4 h^{-1}.[17d]

In comparison, the St-MOP@Pd-2 (0.14 mol% Pd) in this work showed a 92% yield in the visible light-driven Suzuki-Miyaura coupling of 1-acetyl-4-bromobenzene with phenylboronic acid at 25°C after 3 h, corresponding to a TON of 657 and a TOF of 219 h^{-1}. The highly efficient photocatalytic performance of St-MOP@Pd-2 is attributable to its harmony between the efficient visible light-harvesting material (St-MOP) and Pd NPs.

Conclusions

This work shows that Stille coupling reaction provides interesting MOP chemistry. As far as we are aware, St-MOP is the first example of MOP materials based on Stille coupling. First, the size of synthesized St-MOP particles was sensitive to the amount of Pd catalysts and hence could be systematically controlled. As the amount of Pd catalysts increased, the size of St-MOP particles was reduced, which is attributable to enhanced nuclei in the early growth stage. Second, interestingly, Pd NPs were *in situ* deposited on the St-MOP particles to form St-MOP@Pd in one pot. The amount of Pd NPs could be controlled by Pd catalysts. Third, the St-MOP@Pd materials were functional as a visible light-driven photocatalyst. The St-MOP showed visible light absorption at 450 nm and emission at 522 nm. The emission was quenched by Pd NPs, indicating efficient visible light-induced electron transfer from St-MOP to Pd NPs. Among St-MOP@Pd materials, the St-MOP@Pd-2 with an optimal amount of St-MOP and Pd NPs showed efficient photocatalytic activities in the visible light-driven Suzuki-Miyaura coupling. We believe that more various functional MOP materials and new chemistry can be developed based on Stille coupling.

Conflicts of interest

There are no conflicts to declare.

Acknowledgements

This work was supported by the National Research Foundation of Korea (NRF) grant (No. 2020R1A2C200431011) funded by the Korea government (MSIT). K.C.K acknowledges the financial support by Basic Science Research Program (2016R1A6A3A11933303) through the NRF of Korea funded by the Ministry of Education.

Notes and references

1 Reviews: a) B. Zheng, X. Lin, X. Zhang, D. Wu and K. Matyjaszewski, *Adv. Funct. Mater.* 2019, 1907006; b) N. Chaoui, M. Trunk, R. Dawson, J. Schmidt and A. Thomas, *Chem. Soc. Rev.* 2017, **46**, 3302-3321; c) L. Tan and B. Tan, *Chem. Soc. Rev.* 2017, **46**, 3322-3356; d) S. Das, P. Heasman, T. Ben and S. Qiu, *Chem. Rev.* 2017, **117**, 1515-1563; e) Y. Xu, S. Jin, H. Xu, A. Nagai and D. Jiang, *Chem. Soc. Rev.* 2013, **42**, 8012-8031; f) R. Dawson, A. I. Cooper and D. J. Adams, *Prog. Poly. Sci.* 2012, **37**, 530-563; g) F. Vilela, K. Zhang and M. Antonietti, *Energy Environ. Sci.* 2012, **5**, 7819-7832.

2 a) J. -X. Jiang, F. Su, A. Trewin, C. D. Wood, N. L. Campbell, H. Niu, C. Dickinson, A. Y. Ganin, M. J. Rosseinsky, Y. Z. Khimyak and A. I. Cooper, *Angew. Chem. Int. Ed.* 2007, **46**, 8574-8578; b) J.

-X. Jiang, F. Su, A. Trewin, C. D. Wood, H. Niu, J. T. A. Jones, Y. Z. Khimyak and A. I. Cooper, *J. Am. Chem. Soc.* 2008, **130**, 7710-7720.

3 a) Y. Xu, A. Nagai and D. Jiang, *Chem. Commun.* 2013, **49**, 1591-1593; b) W. Zhao, X. Zhuang, D. Wu, F. Zhang, D. Gehrig, F. Laquai and X. Feng, *J. Mater. Chem. A* 2013, **1**, 13878-13884; c) X. Wu, H. Li, B. Xu, H. Tong and L. Wang, *Polym. Chem.* 2014, **5**, 4521-4525; d) R. S. Sprick, J. -X. Jiang, B. Bonillo, S. Ren, T. Ratvijitvech, P. Guiglion, M. A. Zwijnenburg, D. J. Adams and A. I. Cooper, *J. Am. Chem. Soc.* 2015, **137**, 3265-3270; e) B. C. Ma, S. Ghasimi, K. Landfester, F. Vilela and K. A. I. Zhang, *J. Mater. Chem. A* 2015, **3**, 16064-16071; f) H. Ma, B. Li, L. Zhang, D. Han and G. Zhu, *J. Mater. Chem. A* 2015, **3**, 19346-19352; g) P. Pallavi, S. Bandyopadhyay, J. Louis, A. Deshmukh and A. Patra, *Chem. Commun.* 2017, **53**, 1257-1260; h) S. H. Ryu, D. H. Lee, S. M. Lee, H. J. Kim, Y. -J. Ko, K. C. Ko and S. U. Son, *Chem. Commun.* 2019, **55**, 9515-9518.

4 a) L. Sun, Z. Liang, J. Yu and R. Xu, *Polym. Chem.* 2013, **4**, 1932-1938; b) L. Sun, Y. Zou, Z. Liang, J. Yu and R. Xu, *Polym. Chem.* 2014, **5**, 471-478.

5 a) P. Espinet and A. M. Echavarren, *Angew. Chem. Int. Ed.* 2004, **43**, 4704-4734; b) C. Cordovilla, C. Bartolomé, J. M. Martínez-Ilarduya and P. Espinet, *ACS Catal.* 2015, **5**, 3040-3053.

6 C. J. Seechurn, M. O. Kitching, T. J. Colacot and V. Snieckus, *Angew. Chem. Int. Ed.* 2012, **51**, 5062-5085.

7 a) A. Balanta, C. Godard and C. Claver, *Chem. Soc. Rev.* 2011, **40**, 4973-4985; b) M. Pérez-Lorenzo, *J. Phys. Chem. Lett.* 2012, **3**, 167-174; c) A. Biffis, P. Centomo, A. D. Zotto and M. Zecca, *Chem. Rev.* 2018, **118**, 2249-2295.

8 a) S. Ogasawara and S. Kato, *J. Am. Chem. Soc.* 2010, **132**, 4608-4613; b) S. -Y. Ding, J. Gao, Q. Wang, Y. Zhang, W. -G. Song, C. -Y. Su and W. Wang, *J. Am. Chem. Soc.* 2011, **133**, 19816-19822; c) P. Zhang, Z. Weng, J. Guo and C. Wang, *Chem. Mater.* 2011, **23**, 5243-5249; d) N. Huang, Y. Xu and D. Jiang, *Sci. Rep.* 2014, **4**, 7228; e) C. -A. Wang, Y. -W. Li, X. -M. Hou, Y. -F. Han, K. Nie and J. -P. Zhang, *ChemistrySelect* 2016, **1**, 1371-1376; f) C. -A. Wang, -Y. -F. Han, Y. -W. Li, K. Nie, X. -L. Cheng and J. -P. Zhang, *RSC Adv.* 2016, **6**, 34866-34871; g) P. Ju, S. Wu, Q. Su, X. Li, Z. Liu, G. Li and Q. Wu, *J. Mater. Chem. A* 2019, **7**, 2660-2666; h) C. -A. Wang, K. Nie, G. -D. Song, Y. -W. Li and Y. -F. Han, *RSC Adv.* 2019, **9**, 8239-8245; i) W. Xu, C. Liu, D. Xiang, Q. Luo, Y. Shu, H. Lin, Y. Hu, Z. Zhang and Y. Ouyang, *RSC Adv.* 2019, **9**, 34595-34600.

9 Y. Hayashi, *Chem. Sci.* 2016, **7**, 866-880.

10 N. T. K. Thanh, N. Maclean and S. Mahiddine, *Chem. Rev.* 2014, **114**, 7610-7630.

11 a) N. Kang, J. H. Park, M. Jin, N. Park, S. M. Lee, H. J. Kim, J. M. Kim and S. U. Son, *J. Am. Chem. Soc.* 2013, **135**, 19115-19118; b) J. H. Ko, N. Kang, N. Park, H. -W. Shin, S. Kang, S. M. Lee, H. J. Kim, T. K. Ahn and S. U. Son, *ACS Macro Lett.* 2015, **4**, 669-672; c) K. Cho, J. Yoo, H. -W. Noh, S. M. Lee, H. J. Kim, Y. -J. Ko, H. -Y. Jang and S. U. Son, *J. Mater. Chem. A* 2017, **5**, 8922-8926; d) C. W. Kang, J. H. Ko, S. M. Lee, H. J. Kim, Y. -J. Ko and S. U. Son, *J. Mater. Chem. A* 2019, **7**, 7859-7866; e) S. Y. Kang, C. W. Kang, D. W. Kim, Y. Myung, J. Choi, S. M. Lee, H. J. Kim, Y. -J. Ko and S. U. Son, *Chem. Asian J.* 2019, **14**, 3173-3180.

12 P. K. Nayak, S. Mahesh, H. J. Snaith and D. Cahen, *Nature Rev. Mater.* 2019, **4**, 269-285.

13 a) C. K. Prier, D. A. Rankic and D. W. C. Macmillan, *Chem. Rev.* 2013, **113**, 5322-5363; b) K. L. Skubi, T. R. Blum and T. P. Yoon, *Chem. Rev.* 2016, **116**, 10035-10074; c) D. Ravelli, S. Protti and M. Fagnoni, *Chem. Rev.* 2016, **116**, 9850-9913.

14 a) K. Mori, M. Kawashima and H. Yamashita, *Chem. Commun.* 2014, **50**, 14501-14503; b) S. Zhang, C. Chang, Z. Huang, Y. Ma, W. Gao, J. Li and Y. Qu, *ACS Catal.* 2015, **5**, 6481-6488; c) Z. Jiao, Z. Zhai, X. Guo and X. -Y. Guo, *J. Phys. Chem. C* 2015, **119**, 3238-3243; d) A. Xie, K. Zhang, F. Wu, N. Wang, Y. Wang and M. Wang, *Catal. Sci. Technol.* 2016, **6**, 1764-1771; e) G. Singh, M. Kumar, K. Sharma and V. Bhalla, *Green Chem.* 2016, **18**, 3278-3285; f) D. Sun and Z. Li, *J. Phys. Chem. C* 2016, **120**, 19744-19750; g) H. H. Shin, E. Kang, H. Park, T. Han, C. -H. Lee and D. -K. Lim, *J. Mater. Chem. A* 2017, **5**, 24965-24971; h) S. Roslin and L. R. Odell, *Chem. Commun.* 2017, **53**, 6895-6898; i) Y. Luo, Y. Peng, W. Liu, F. Chen and B. Wang, *Chem. Eur. J.* 2017, **23**, 8879-8885; j) M. Koohgard and M. Hosseini-Sarvari, *Catal. Commun.* 2018, **111**, 10-15; k) M. Hosseini-Sarvari and Z. Bazyar, *ChemistrySelect* 2018, **3**, 1898-1907; l) R. Duarah and N. Karak, *Ind. Eng. Chem. Res.* 2019, **58**, 16307-16319.

15 a) X. Huang, Y. Li, Y. Chen, H. Zhou, X. Duan and Y. Huang, *Angew. Chem. Int. Ed.* 2013, **52**, 6063-6067; b) F. Wang, C. Li, H. Chen, R. Jiang, L. -D. Sun, Q. Li, J. Wang, J. C. Yu and C. -H. Yan, *J. Am. Chem. Soc.* 2013, **135**, 5588-5601; c) S. Sarina, H. Zhu, E. Jaatinen, Q. Xiao, H. Liu, J. Jia, C. Chen and J. Zhao, *J. Am. Chem. Soc.* 2013, **135**, 5793-5801; d) Q. Xiao, S. Sarina, A. Bo, J. Jia, H. Liu, D. P. Arnold, Y. Huang, H. Wu and H. Zhu, *ACS Catal.* 2014, **4**, 1725-1734; e) Q. Xiao, S. Sarina, E. Jaatinen, J. Jia, D. P. Arnold, H. Liu and H. Zhu, *Green Chem.* 2014, **16**, 4272-4285; f) J. Guo, Y. Zhang, L. Shi, Y. Zhu, M. F. Mideksa, K. Hou, W. Zhao, D. Wang, M. Zhao, X. Zhang, J. Lv, J. Zhang, X. Wang and Z. Tang, *J. Am. Chem. Soc*. 2017, **139**, 17964-17972; g) S. Rohani, A. Ziarati, G. M. Ziarani, A. Badiei and T. Burgi, *Catal. Sci. Technol.* 2019, **9**, 3820-3827.

16 X. -H. Li, M. Baar, S. Blechert and M. Antonietti, *Sci. Rep.* 2013, **3**, 1743.

17 a) Z. J. Wang, S. Ghasimi, K. Landfester and K. A. I. Zhang, *Chem. Mater.* 2015, **27**, 1921-1924; b) Y. Gu, J. Li, A. Xie, K. Zhang, Y. Jiao and W. Dong, *Catal. Sci. Technol.* 2018, **8**, 5201-5206; c) J. Chakraborty, I. Nath and F. Verpoort, *Chem. Eng. J.* 2019, **358**, 580-588; d) B. Guo, H. -X. Li, C. -H. Zha, D. J. Young, H. -Y. Li and J. -P. Lang, *ChemSusChem* 2019, **12**, 1421-1427.

18 V. Blum, R. Gehrke, F. Hanke, P. Havu, V. Havu, X. Ren, K. Reuter and M. Scheffler, *Comput. Phys. Commun*. 2009, **180**, 2175-2196.

19 J. F. Moulder, W. F. Stickle, P. E. Sobol and K. D. Bomben, *Handbook of X-ray Photoelectron Spectroscopy*, *Physical Electronics*, Inc., 1995

20 K. Suzuki, A. Kobayashi, S. Kaneko, K. Takehira, T. Yoshihara, H. Ishida, Y. Shiina, S. Oishi and S. Tobita, *Phys. Chem. Chem. Phys.* **2009**, *11*, 9850-9860.

21 A. Suzuki, *J. Organomet. Chem*. 1999, **576**, 147-168.

View Article Online
DOI: 10.1039/D0CY00997K

Table of Contents

Stille coupling results in the *in situ* deposition of Pd NPs on microporous organic polymer, showing excellent performance in the visible light-driven Suzuki-Miyaura coupling.